Extending refractory lifetime in rotary kilns for hazardous waste incineration

Adrian Villalba Weinberg, Cyrille Varona, Xavier Chaucherie, Dominique Goeuriot, Jacques Poirier

HAL Id: emse-01493380

https://hal-emse.ccsd.cnrs.fr/emse-01493380v1

Submitted on 22 Apr 2024

Author's Accepted Manuscript

Extendingre fractory lifetime in rotary kilns for hazardous waste incineration

Adrian Villalba Weinberg, Cyrille Varona, Xavier Chaucherie, Dominique Goeuriot, Jacques Poirier
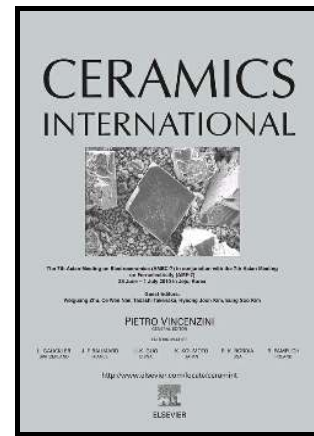
Cite this article as: Adrian Villalba Weinberg, Cyrille Varona, Xavier Chaucherie, Dominique Goeuriot and Jacques Poirier, Extendingre fractory lifetime in rotary kilns for hazardous waste incineration, *Ceramics International,* http://dx.doi.org/10.1016/j.ceramint.2016.08.078

Extending refractory lifetime in rotary kilns for hazardous waste incineration

Adrian Villalba Weinberg[a,c,d], Cyrille Varona[a], Xavier Chaucherie[b], Dominique Goeuriot[c], Jacques Poirier[d]

[a]BONY SA – Produits réfractaires, 53 Boulevard Fauriat, 42000 Saint-Étienne, France

[b]SARPI–VEOLIA, 427 Route du Hazay, 78520 Limay, France

[c]LGF CNRS UMR 5307, MINES Saint-Étienne, 158 Cours Fauriel, 42023 Saint-Étienne, France

[d]CEMHTI CNRS UPR 3079, Université d'Orléans, 1D Avenue de la Recherche Scientifique, 45071 Orléans, France

adrian.villalba-weinberg@cnrs-orleans.fr

c.varona@bony-sa.fr

xchaucherie@sarpindustries.fr

dgoeuriot@emse.fr

jacques.poirier@univ-orleans.fr

Abstract

The main costs for modern rotary kiln incinerators are refractory brick maintenance. Every 1-3 years, parts or the entire brick lining has to be renewed due to refractory wear and tear. Often, the blame is laid on thermo-chemical corrosion. To reassess this prevailing dogma, a comprehensive wear mechanism was elaborated that includes the impact of bottom ash characteristics at operating temperatures. Thermodynamic calculations were employed as well as a post-mortem analysis of refractory bricks from three rotary kilns. Changes in chemical and mineralogical composition and microstructure were examined. Surprisingly, results show that there is no significant thermo-chemical reaction between refractory material and the molten bottom ash. In fact, the melt penetrates open pores by capillary action up to 5 mm in depth. Under this infiltrated zone, serious cracks are systematically visible in all type of bricks. We suspect a mismatch of thermal expansion coefficients to be the cause of crack initiation. These cracks lead finally to spalling of degraded refractory layers. Therefore, refractory materials used nowadays are not optimal. To conclude, experimental based guidelines are provided that may help operators extend the lifetime of the refractory bricks and reduce maintenance cost significantly.

1. Introduction

1.1. Hazardous waste incineration

Hazardous wastes include pesticides, oils, waste fuels, acids, filter cakes and aerosols to name but a few. The rotary kiln is the state-of-the-art technology to incinerate hazardous wastes thanks to its high capacity (up to 120,000 t/y) and versatility [1,2]: Rotary kilns are able to treat solid, pasty and liquid wastes all together. Typical kilns are from 5 to 15 m long with diameters from 3 to 5 m. The co-current flow design is standard, where wastes and gas flow in the same direction. Solid wastes reach the kiln through a feed chute on a stationary front wall (Fig. 1). Liquid wastes are injected through nozzles placed next to the chute. In order to withstand extreme temperatures and molten bottom ash, the whole inner kiln is protected by a thermal & resistant barrier composed of dense refractory bricks. The kiln is slightly inclined (~3 %) and rotates with 0.05-0.7 rpm, resulting in a mean residence time of 30-90 min for solid and pasty wastes [1]. Wastes transform into gas and bottom ash, a liquid/solid mineral residue that falls at the kiln outlet into a water tank. Gas leaving the rotary kiln towards the secondary combustion chamber has a fairly high oxygen content (7-10 %) [3]. Nevertheless, reducing conditions may prevail near the bed region [4].

Two philosophies coexist on how to run the rotary kiln: ashing or slagging modes. The effect on refractory disintegration differs because mean temperatures are 850-1150 °C in ashing mode and 1100-1400 °C in slagging mode [5–7]. Consequently, the viscosity and corrosiveness of the combustion residue are not the same.

Most rotary kiln incinerators in Europe operate in ashing mode, as the overall operating costs turned out to be lower than in slagging mode. All rotary kilns presented in this work run in ashing mode as well.

Fig. 1 shows a typical temperature profile inside the kiln, at the hot face of the refractory lining. It is important to mention that the mean temperature shown in fig. 1 does not reveal temperature fluctuations due to varying waste inputs. Temperature peaks up to 1400 °C and dropdowns to 700 °C are indeed common in ashing kilns. Another specific aspect of rotary kilns is temperature cycling induced by rotation: In contact with the flame of burning wastes, the temperature at the refractory's hot face is at least

1200 °C but declines below 900 °C while the brick is far from the flame. Every kiln rotation provokes therefore a temperature change of more than 300 °C.

1.2. Statement of the problem

The critical problem of rotary kiln incineration is high maintenance cost caused by refractory wear. A typical refractory lifetime is from 1‑3 years. High costs arise not only from the purchase of the refractory products, but, most notably from the work stoppage of the kiln during the lining's replacement.

Previous work has tried to increase refractory durability by (a) changing operating conditions [7,8] or (b) improving the refractory material [9,10]. In the former, the idea is to control viscosity of the bottom ash in order to protect the refractory lining against wear by building up a protective deposit of solidified bottom ash that sticks to the lining. This method has become common practice. Many plant operators air or water cool the external steel shell in order to thicken the deposit layer, enhancing thereby the refractory's lifetime [1]. Nevertheless, the inhomogeneous temperature profile throughout the kiln leads to inhomogeneous layer thicknesses. As a result, refractory bricks are less protected in the inlet and outlet zones and therefore more susceptible to wear. Since it is almost impossible to adjust temperature in the different kiln zones, an attempt should be to adjust the chemical composition of the bottom ash. At first glance, this endeavor might seem unpromising in view of the broad range of wastes that are incinerated. Yet, the opposite is actually the case: The composition of the inorganic residue is rather stable. What operators need are simple rules of thumb to exert influence on melting behavior.

As to optimizing materials, much effort has been done to extend operating life [9–11]. According to laboratory corrosion tests, bauxite based bricks and alumina-chromia bricks containing 5-15 wt% Cr_2O_3 have turned out to better withstand molten bottom ash and alkalis at high temperatures. For that reason, bauxite and alumina-chromia became the materials chosen for modern rotary kiln incinerators. However, that research concentrated on corrosion, as it was perceived to be the main cause of failure. The limited improvement on refractory lifetime shows that the wear mechanism is still little understood.

1.3. Aim of this work

Our objective is to study and discover the actual wear mechanism of the refractory material. To understand the wear mechanism, it is advantageous to begin with the bottom ash characteristics at operating temperatures, since bottom ash is in direct contact with the refractory and interacts with it. We

will highlight viscosity, as it is the key parameter to build a deposit layer that sticks to the refractory lining and protects it. Indeed, main focus will be placed on the examination of used refractory bricks from three rotary kiln incinerators. Microstructural changes together with bottom ash characteristics will form the basis to develop a coherent wear mechanism.

This knowledge will both help incinerator operators to choose an appropriate refractory material and provide material scientists and engineers with ideas to develop novel, custom-tailored materials with higher performances.

2. Experimental procedure

2.1. Characterization methods

The melting behavior of bottom ash was investigated by thermodynamic calculations and verified by laboratory tests. Solidus and liquidus temperatures of bottom ashes were calculated with FactSage®, a thermodynamic database computing software. Databases FactPS for pure substances and FToxid for oxides, both updated in 2013, were applied. In order to speed up calculations, only oxides > 2 wt% were included. Iron oxide was considered half (molar) as FeO, the other half as Fe_2O_3, as Fe_3O_4 was the most common phase in bottom ashes. Viscosities of liquid phases were calculated with FactSage® as well, using viscosity database "glasses", which is valid for the whole temperature range. The viscosity program calculates structural units and then uses the Modified Quasichemical Model to predict the viscosity of the melt [12]. Nota bene: P_2O_5 could not be included into the calculations, because it was not incorporated in the viscosity program's database.

In order to compare calculations with actual softening behavior, pill tests at different temperatures were carried out. Bottom ash pellets of 13 mm diameter and 3 mm height were obtained by pressing 0.75 g dried and milled bottom ash at 100 MPa. Pellets were placed on slices of refractory material M1 and heated under oxidizing atmosphere (air) with 5 °C/min until 1000 °C (dwell time 5h). This heating cycle was repeated in 50 °C steps until 1200 °C. Photos were taken after each thermal treatment.

Failure analysis consisted of macroscopic and microscopic observations. A slice of 10 mm thickness was cut out from the middle of each used brick by means of a water-cooled diamond saw. Cut slices were photographed to document large cracks. Possible microstructural changes were examined with a scanning electron microscope Hitachi S-4500 on polished and carbon metallized samples taken from the refractory's hot face.

In order to reveal possible phase transformations, X-ray powder diffraction (XRD) was conducted on $(5\times5\times10)$ mm^3 samples cut out from used and unused bricks. Samples were grinded to powder beforehand and analyzed with a Bragg-Brentano diffractometer (D8 Advance, Bruker, Germany) using Cu Kα radiation.

X-ray diffraction is an adequate method to analyze crystallographic phases, but not amorphous samples. Therefore, X-ray fluorescence measurements were chosen to be used on specimens at different distances from the deposit/brick interface. 1 g of each sample powder was mixed with 5 g of glass forming agent $Li_2B_4O_7$. The mixture was heated to 1100 °C inside a platinum crucible in an electric fluxer (K1, Katanax, Canada). The melt was casted to a pellet to be analyzed quantitatively in an X-ray fluorescence analyzer (EDX-720, Shimadzu, Japan). The chemical compositions of bottom ashes were obtained in the same manner after having burned residual organics at 450 °C and grinded the dried residue.

2.2. Bottom ashes

Bottom ashes from three rotary kiln incinerators (RK1-3) were analyzed with regard to chemical and mineralogical composition. Additionally, a synthesized bottom ash, named SYNTH, was prepared. SYNTH embodies a simplified model system and is close to the mean composition of real bottom ashes. This model system was limited to the five most important oxides: SiO_2, CaO, Fe_2O_3, Al_2O_3 and Na_2O. Compared to the actual bottom ashes, Na_2O and CaO contents in SYNTH were slightly increased to compensate the absence of fluxing oxides K_2O and MgO. Composition SYNTH is well suited for thermodynamic calculations and behaves in corrosiveness and viscosity like real bottom ashes. Chemical compositions are given in Tab. 1. In this table, iron oxide is assumed to be fully oxidized, i.e. as Fe_2O_3, as it is commonly done in the literature. Yet, iron oxide may be occasionally not fully oxidized, i.e. in form of Fe_3O_4 or even FeO, if organics and metals are still present in the bottom ash, producing locally reducing conditions.

2.3. Rotary kilns and their refractory linings

In total, 17 used bricks were recovered from three rotary kilns. Rotary kiln RK2 delivered bricks from inlet, combustion and outlet zones of the kiln. RK1 and RK3 only delivered bricks from combustion and outlet zones. The three kilns represent typical French incineration practice – in terms of kiln size and waste inputs. Kilns are 13.5 m, 12.0 m and 7.8 m long for RK1, RK2 and RK3 respectively and their

inner kiln diameters are 3.9 m, 4.0 m and 2.5 m wide. All these kilns are not insulated, i.e. the working lining is in direct contact with the steel shell.

In general, refractory bricks have a fine-grained matrix in which grog aggregates (grain sizes 0.1-5 mm) are embedded. The porous matrix contains the bonding phase made of fine powders (grain sizes < 0.1 mm). Three standard refractory products were dealt with: a high alumina refractory material M1 based on bauxite, an alumina-chromia refractory material M2 containing 5 wt% Cr_2O_3 and another alumina-chromia refractory material M3 containing 10 wt% Cr_2O_3. Natural raw materials bauxite and clay used for M1 are responsible for the presence of secondary oxides Fe_2O_3, TiO_2 and MgO and for its higher porosity (Tab. 2). Thanks to its lower porosity and the strong bonding phase, materials M2 and M3 exhibit extremely high cold crushing strengths (CCS) of 160 MPa and 180 MPa. As a result, materials M2 and M3 should resist abrasion better than M1. However, thermal expansion plays an important role to withstand thermal shocks. Here, material M1 has a plus over M2 and M3. Despite these differences, all materials contain > 78 wt% Al_2O_3 and are designed to withstand corrosion at high temperatures. When it comes to resistance against thermal shocks and cycling, all these materials are not optimal.

3. Results and discussion

3.1. Melting behavior of bottom ashes

Fig. 2 illustrates the melting behavior of bottom ash SYNTH. When heating, first liquid phases appear reaching solidus temperature T_{sol}, at about 950 °C. Then the solid/liquid interval begins. Finally, liquidus temperature T_{liq} is reached at about 1350 °C, where bottom ash becomes entirely liquid. Cooling down from the liquid state, iron oxide and iron containing phases precipitate first, followed by CaO-rich phases. In actual conditions, molten bottom ash has limited time to solidify and therefore crystallizes only partially. The silica-rich liquid solidifies mostly to an amorphous phase due to its high viscosity. This amorphous phase contains about 45 wt% SiO_2, 25 wt% CaO, 10 wt% Al_2O_3, all alkali oxides accessible and to a smaller extent Fe_xO_y and TiO_2. The major parts of Fe_xO_y and TiO_2 form solid crystals that are dispersed in the amorphous phase.

3.1.1. Viscosity

The key parameter that controls deposit formation is viscosity. Three factors govern viscosity: chemical composition of the liquid phase, fraction of solid particles, and temperature. In the melting interval T_{sol}-

6

T_{liq}, the liquid phase contains solid, iron-rich, crystals. The question arises: How do the solid particles influence the overall viscosity of the suspension? For all ranges of solid percentages, Krieger proposed equation eq. 1 [13,14].

$$\eta_{eff} = \eta_{liq}(1 - (f/f_c))^{-Bf_c}$$ Eq. 1

Herein, the effective viscosity η_{eff} of the suspension depends on the viscosity η_{liq} of the liquid phase, the volume fraction f of the solid particles, a limit value f_c for the solid fraction and a constant B depending on the particles' geometry. In case of uniform spheres, B equals 2.5 and the limit value for the volume fraction can be set at f_c=0.62, which corresponds to the solid volume fraction of randomly packed spheres. Viscosity η_{liq} of the liquid phase follows a complex curve that is calculated with FactSage®.

Two reference points are of interest to evaluate the absolute viscosity values: a threshold at which the bottom ash starts to stick to the refractory material and another threshold under which the liquid phase starts to penetrate the material. For the former threshold, it stands to reason to use the softening point of glass, i.e. the point where glass deforms under its own weight, which is fixed at $10^{6.6}$ Pa·s [15]. Determining the viscosity value at which the liquid phase starts to infiltrate the material is a far more difficult task, because it depends on viscosity, but also on the material parameters of the refractory, i.e. porosity, pore size distribution, wetting angle and interface tension. The penetration depth l of a liquid into a porous material with pore radius r (average pore diameters of the refractory materials are given in tab. 2) can be described by the Washburn equation (Eq. 2) [16].

$$l = \sqrt{\frac{\gamma cos\theta}{2\eta}rt}$$ Eq. 2

Wherein γ is the interface tension, θ the wetting angle between refractory material and infiltrating liquid, and t the time.

By increasing the temperature, the infiltrating liquid will undergo a viscosity drop of several orders of magnitude, whereas interface tension will not change much. Skupien and Gaskell measured the surface tension of a $CaO-FeO-SiO_2$ melt with 30 wt% FeO and different CaO/SiO_2 ratios to be 0.3-0.5 N/m at 1300-1400 °C [17]. Interestingly, surface tension was barely affected by temperature, which emphasizes that in our case the interface tension is not the dominating parameter. The wetting angle is influenced by viscosity; high viscosities will normally lead to high wetting angles. Therefore, in order to simplify matters, we focus only on viscosity, as it is in our case the determining factor. The infiltration threshold was set at 10^3 Pa·s. To give you a better idea, the viscosity of water at room temperature is 1 Pa·s and of honey 10^4 Pa·s.

Fig. 3 shows the change of the effective viscosity with temperature, calculated with the formerly mentioned values for f_c and B and the simplification of replacing the volume fraction f by the mass fraction. At low temperatures (~1000 °C), high solid fractions increase drastically the effective viscosity. Contrary, at high temperatures (> 1200 °C), solid fraction is low; thus, its influence on viscosity is marginal.

3.1.2. The concept of basicity

A practical way to predict melting behavior by means of slag composition is the concept of basicity, which has been originally developed by metallurgists [18]. The concept is based on the polymerization degree of a molten mass, i.e. the bond network between the constituents. The more chains are present, the more viscous the melt is. Basicity is expressed as the molar ratio between glass modifier oxides (chain breakers), like CaO, and glass-forming oxides, like SiO_2. As a rule of thumb, higher basicities lead to lower viscosities of the liquid part but also to higher melting temperatures. Lower basicities have the adverse effect of increasing viscosity and reducing melting temperature. There are different definitions of basicity, from easy manageable to complex and more precise models [18]. The present work proposes eq. 3 to determine the basicity of the bottom ashes. This basicity index was used by Senior and Srinivasachar to predict the viscosity of coal ashes [19]. Since coal ashes are chemically close to bottom ashes, it seems legitimate to use this equation for our purpose. The basicity index was extended with P_2O_5. Note: P_2O_5 forms, similar to SiO_2, bridging oxygen bonds [20] and is therefore a strong glass forming oxide that must be considered as it often attains noticeable percentages in bottom ashes.

$$\frac{CaO+MgO+FeO+Na_2O+K_2O-Al_2O_3-Fe_2O_3}{\frac{SiO_2+TiO_2+P_2O_5}{2}+Al_2O_3+Fe_2O_3} \qquad \text{Eq. 3}$$

The role of iron oxide depends on iron's degree of oxidation, which, in return, depends on the atmosphere present. We will consider one molar half as FeO, the other half as Fe_2O_3, since XRD measurements of the bottom ashes revealed Fe_3O_4 (=$FeO \cdot Fe_2O_3$) to be the most common degree of oxidation.

3.1.3. Practical relevance of basicity and viscosity

To verify the theoretical concept of basicity, laboratory pill tests at different temperatures were carried out (Fig. 4). The heuristic predicts the highest melting temperature for the bottom ash with the highest basicity, RK1, which is in fact the case. Once the softening temperature is reached at 1100-1150 °C, the liquid diffuses immediately over the entire refractory sample due to its low viscosity. Contrary, the

bottom ash with the lowest basicity, RK3, begins already to soften at 1000-1050 °C and viscosity decreases gradually.

A comparison of basicity and viscosity demonstrates the practical relevance of basicity (compare fig. 4 and fig. 3). The adhesion threshold of the effective viscosity η_{eff} correlates well with the softening point of the pill tests. Furthermore, the bottom ash with the highest basicity, RK1, produces the liquid phase with the lowest viscosity η_{liq}, able to infiltrate the material at 1125 °C. However, a high basicity leads also to higher fractions of solid particles, increasing effective viscosity η_{eff}, thus, shortening the temperature range, in which a deposit can build up. Contrary, bottom ashes with low basicities have the dual advantage to form deposits over a larger temperature interval and to reduce infiltration.

3.2. Post-mortem analysis of refractories

3.2.1. Macro- and microstructural changes

Transversal cuts of representative bricks (Fig. 5) spotlight the dark deposit layer of solidified bottom ash sticking to the hot facing side of the bricks. Bricks in the combustion zone are covered by a thicker deposit layer, which provides better protection and leads to higher final brick thicknesses. In the outlet zone, deposit thicknesses decrease, and consequently final brick thicknesses decrease as well. This is because these bricks are less protected against thermal shocks and cycling. The fastest degradation is observed at the beginning of the outlet zone, where wear rates attain 8 mm/month (RK1), 9 mm/month (RK2) and 14 mm/month (RK3). High wear is also observed in the first meters of RK2, where generally deposits develop difficultly. The absence of the deposit layer can be related to waste inputs with high moisture contents or low calorific values. Without a deposit layer, bricks are directly exposed to thermal shocks by cold liquid wastes dropping on the hot refractory material. Hence, an excessive injection of low calorific liquid wastes has a twofold negative impact: First, this hinders the formation of a protective deposit layer and second, provokes thermal shocks when they drop on the hot refractory lining.

Apparently, employment of materials M1, M2 or M3 has no significant impact on the wear profile. Different products placed next to each other, e.g. in RK3, M2 at 4.5 m and M3 at 5.5 m, show similar final brick thicknesses.

In material M3, a yellow water soluble salt composed of potassium and chromium indicates that toxic potassium chromate K_2CrO_4 was formed by a chemical reaction between the chromia containing refractory and potassium from the bottom ash or the kiln atmosphere. Hexavalent chromium compounds,

as K_2CrO_4, are a serious health risk for those workers in contact with the contaminated bricks over normally a one-week period when removing the worn lining. After all, there are about 8,000 bricks involved when replacing the entire lining of the kiln.

When a closer look is taken at the bricks, severe cracks are revealed (Fig. 6). Most cracks grew parallel to the hot face, a few millimeters from the deposit/brick interface. Indeed, all three materials are susceptible to crack formation, but in the chromia-containing materials M2 and M3, cracks appear even larger. Cracks in bauxite based material M1 are smaller but more numerous, which is a sign of both a better crack growth resistance combined with a poorer resistance to crack initiation.

Micrographs obtained by scanning electron microscopy make clear that cracks grew through the matrix and not through aggregates (Fig. 7). The micro-cracked matrix is systematically located behind an infiltrated zone. Molten bottom ash infiltrated the matrix up to 5 mm depth via a tunnel network of open pores and cracks. Apparently, the high viscosity of the infiltrating liquid limited deeper infiltration into the material. Degradation is obviously linked to the macro-cracks observable by the naked eye – such cracks lead to spalling of refractory layers. However, spalling due to macro-cracks occurs only at the end-stage of a sequence: initial crack formation → crack growth → cross-linking of micro-cracks → growth of macro-cracks → spalling of refractory layers. Understand, cracks are triggered by stresses. Some stresses can arise from thermal shocks or thermal cycling due to the kiln rotation. Additional stresses can be caused by an altered microstructure through infiltration and/or chemical reaction at the refractory's hot face, which will be investigated in the section that follows.

3.2.2. Chemical and mineralogical changes

With the exception of Na_2O, most bottom ash components penetrate the matrix until 2.5 mm to 7.5 mm depth (Fig. 7-9). Behind this infiltrated zone, oxide percentages are kept at a constant level, corresponding to the original refractory material. Although bottom ashes contain only 5 wt% Na_2O, Na_2O reaches deeper into the material (until 7.5-12.5 mm) than other oxides, because of its fluxing ability: The first melts that appear when heating bottom ash are alkali-rich. Additionally, at higher temperatures, these alkali-rich melts are more fluid. The EDS analysis in fig. 7 shows that the penetrating melt is richer in alkaline and alkaline earth oxides and much poorer in Fe_xO_y than the mean bottom ash composition. The reason is that solid particles (Fe- and Ti-rich) and highly viscous melts (poor in CaO and alkalis) remain at the surface, as they are not able to pass through the narrow pore network.

Dissolution of the refractory material by the penetrating melt is expected to be insignificant, since diffusion inside a highly viscous liquid is presumably slow. The dependence of the diffusion coefficient D of a component through a liquid with viscosity η is described by the Stokes-Einstein relation (Eq. 4) [21].

$$D = \frac{k_B T}{6\pi\eta r} \qquad \text{Eq. 4}$$

Where k_B is Boltzmann's constant and r the radius of the diffusing particle. Thereafter, only during temperature peaks, when viscosity is low enough, refractory components are likely to be dissolved by the penetrating liquid.

Whether the molten mass reacts chemically with the refractory brick or not, is answered by X-ray diffraction patterns, shown in fig. 10-12. Surprisingly, after 21 months in service, material M1 was unaffected by chemical attack. There are no new phases in the infiltrated zone emerging from interactions between bottom ash and refractory material. The sole new phase is cristobalite (SiO_2). This phase is not the result of corrosion, but of slow phase transformation from amorphous silica towards cristobalite that is at service temperature in thermodynamic equilibrium. However, cristobalite is not the cause of crack formation.

A similar case was observed in material M2. The infiltrating liquid does not react with bottom ash constituents. The only change is the disappearance of the $AlPO_4$ peak. This slight phase transformation cannot be attributed to the crack formation, either.

In material M3, same phases are present as in the original material. Corundum (Al_2O_3), eskolaite (Cr_2O_3) and baddeleyite (ZrO_2) are all stable at kiln operating temperatures. Thus, they do not transform into other phases. The presence of K_2CrO_4 that was observable by the naked eye (Fig. 6), is too low to be visible in the XRD patterns.

3.3. Wear mechanism

X-ray patterns have shown that there is no evidence for alkali attack or any chemical reaction. Therefore, corrosion cannot be the cause of failure. Liquid phases from the bottom ash infiltrate the porous matrix indeed, but operating temperatures are too low to enable thermo-chemical reactions with the refractory material.

Large cracks argue for a wear mechanism based on consecutive spalling of refractory layers, as illustrated in fig. 13. Cracks grow right behind the infiltrated zone, at about 5 mm from the deposit/brick interface. A mismatch of thermal expansion behavior between infiltrated and non-infiltrated material may be the

reason for the crack formation. The infiltrating liquid closes pores and transforms at lower temperatures to a glass-like, solid phase that alters the properties of the material.

Spalling is observed in the entire kiln, but the spalling mechanism differs in the various kiln zones (Fig. 14). Near the inlet, wastes have not yet transformed into bottom ash. Therefore, a protective bottom ash layer is often absent. Bricks are thereby exposed to harsh thermal shocks by relatively cold liquid wastes dropping on the hot bricks. Results are cracking and spalling of refractory layers.

In the beginning of the combustion zone, bottom ash forms a thick deposit, thanks to sufficiently high mean temperatures. At ordinary operating temperatures, this deposit stays solid or highly viscous and protects the refractory material. However, at temperature peaks (> 1150 °C), viscosity reduces and the liquid phase penetrates via open pores into the matrix. Fortunately, the thick deposit layer acts as a thermal barrier and keeps stresses low at the interface between infiltrated and non-infiltrated zone. Therefore, spalling is reduced and wear rate is slowed in this kiln zone.

In the second half of the kiln, the deposit thickness diminishes, as effective viscosity η_{eff} of the bottom ash is too high to make sticking possible. Yet, at temperature peaks, the liquid phase with viscosity η_{liq} still infiltrates the brick lining. Thermal cycling due to the kiln's rotation provokes crack formation at the interface between infiltrated and non-infiltrated zones and leads finally to spalling of infiltrated layers.

4. Conclusions

Wear of the refractory lining in rotary kiln incinerators running in ashing mode is governed by spalling, not corrosion. Nevertheless, bottom ash plays a major role in the degradation process – both positively and negatively: The partially molten ash may build a protective deposit layer or penetrate the refractory material promoting spalling.

Longer refractory brick lifetimes can be achieved by two approaches: (a) Depositing a solidified bottom ash throughout the kiln by controlling viscosity. Or (b) by choosing a more resistant refractory material.

4.1. How to control bottom ash viscosity

Bottom ash does not form a protective deposit layer unless temperature reaches 1050 ± 50 °C. Bottom ash only then is viscous enough to stick to the lining. In terms of viscosity, η_{eff} of the bottom ash should be kept under $10^{6.6}$ Pa·s to enable adhesion between brick and bottom ash. However, viscosity η_{liq} of the

liquid phase should be maintained higher than 10^3 Pa·s to avoid penetration and degradation of the refractory bricks. The following advices help to realize this.

1. Basicity of bottom ash should be monitored regularly

2. High basicities (> 1.0) should be avoided as they displace deposit formation towards higher temperatures and increase infiltration

3. Silica-rich bottom ashes with low basicities (< 0.5) are desirable, as they promote deposit formation and decrease infiltration. SiO_2-rich additives to the solid waste, e. g. crushed glass, are a possibility to reduce basicity and improve the melting behavior

4. Alkali-rich wastes should be incinerated at low temperatures to avoid fluxing of the deposit

5. Cooling the second half of the kiln by ventilators or water jackets at the outer steel shell helps to diminish infiltration

4.2. How to select appropriate refractory materials

Refractory materials used nowadays are designed to withstand high temperatures and chemical attack. Both are not the case in rotary kiln incinerators running in ashing mode. The most important aspect when choosing a refractory product is spalling resistance. Bauxite and alumina-chromia bricks are not the best option due to high thermal expansion and high mechanical strengths. Chromia-containing products have the additional drawback of forming harmful chromium(VI) compounds. Refractory materials based on andalusite should resist better thanks to its crack deflection and crack healing behavior [22].

Second crucial factor is infiltration resistance. Here, porosity plays an important role. Lower porosities and lower pore sizes are preferred in order to restrain liquid phases from infiltrating the refractory.

References

[1] IPPC Bureau, Reference document on the best available techniques for waste incineration. http://eippcb.jrc.ec.europa.eu/reference/, 2006 (accessed 23.03.2016).

[2] H. Freeman, R. Olexsey, D. Oberacker, R. Mournighan, Thermal destruction of hazardous waste— a state-of-the-art review, J. Hazard. Mater. 14 (1987) 103–117.

[3] J. Bujak, Determination of the optimal area of waste incineration in a rotary kiln using a simulation model, Waste Manage. 42 (2015) 148–158.

[4] Y. Yang, M.J. Pijnenborg, M.A. Reuter, J. Verwoerd, Modeling the combustion behavior of hazardous waste in a rotary kiln incinerator, J. Environ. Sci. Heal. A. 40 (2005) 1823–1842.

[5] V. Cundy, T. Lester, C. Leger, G. Miller, A. Montestruc, S. Acharya, A. Sterling, D. Pershing, J. Lighty, G. Silcox et al., Rotary kiln incineration—combustion chamber dynamics, J. Hazard. Mater. 22 (1989) 195–219.

[6] J.M. Veranth, D. Gao, G.D. Silcox, Field investigation of the temperature distribution in a commercial hazardous waste slagging rotary kiln, Environ. Sci. Technol. 30 (1996) 3053–3060.

[7] B. Vosteen, J. Beyer, T. Boukhofer, Simultaneous inner and outer thermography of rotary kilns for hazardous waste incineration—controlled protective slagging results in a considerable prolongation of refractory life, VGB Powertech 82 (2002) 71–77.

[8] P.B. Queneau, D.E. Cregar, L.J. Karwaski, Slag control in rotary kiln, Pollut. Eng. 24 (1992) 26– 32.

[9] J.A. Caprio, H.E. Wolfe, Refractories for hazardous waste incineration—an overview, in: Proc. ASME National Solid Waste Processing Conf., New York, 1982: pp. 139–159.

[10] J. Sperber, R. Burgard, F.-J. Duennes, Innovative lining concepts for hazardous waste incineration, Refractories Worldforum 4 (2012) 85–98.

[11] L. Bly, R. Pena, Waste incineration—some background and furnace refractory design review, in: Proc. UNITECR'89, 1989: pp. 980–993.

[12] A.N. Grundy, H. Liu, I.-H. Jung, S.A. Decterov, A.D. Pelton, A model to calculate the viscosity of silicate melts, J. Mater. Res. 99 (2008) 1185–1194.

[13] I.M. Krieger, Rheology of monodisperse latices, Adv. Colloid. Interface. Sci. 3 (1972) 111–136.

[14] W. Pabst, Fundamental considerations on suspension rheology, Ceram. Silik. 48 (2004) 6–13.

[15] J.E. Shelby, Introduction to glass science and technology, 2nd ed., Royal Society of Chemistry, 2005.

[16] E.W. Washburn, The dynamics of capillary flow, Phys. Rev. 17 [3] (1921) 273–283.

[17] D. Skupien, D. Gaskell, The surface tensions and foaming behavior of melts in the system CaO-FeO-SiO$_2$, Metall. Mater. Trans. B 31 (2000) 921–925.

[18] M. Allibert, Slag Atlas, Verlag Stahleisen, 1981.

[19] C.L. Senior, S. Srinivasachar, Viscosity of ash particles in combustion systems for prediction of particle sticking, Energy & Fuels 9 (1995) 277–283.

[20] B.O. Mysen, F.J. Ryerson, D. Virgo, The structural role of phosphorus in silicate melts, Am. Mineral. 66 (1981) 106–117.

[21] J.T. Edward, Molecular volumes and the Stokes-Einstein equation, J. Chem. Educ. 47 [4] (1970) 261–270.

[22] M.-L. Bouchetou, J.-P. Ildefonse, J. Poirier, P. Daniellou, Mullite grown from fired andalusite grains: the role of impurities and of the high temperature liquid phase on the kinetics of mullitization and consequences on thermal shocks resistance, Ceram. Int. 31 (2005) 999–1005.

Fig. 1. Schematic drawing of the combustion process in a rotary kiln incinerator and mean temperatures at the refractory's hot face measured at SARPI-VEOLIA incineration plant RK2.

Fig. 2. Equilibrium phases at different temperatures and normalized composition of the liquid phase. Calculated with FactSage® for bottom ash SYNTH.

Fig. 3. Viscosities η_{liq} (grey lines) of liquid phases calculated with FactSage® and effective viscosities η_{eff} (black lines) according to Krieger.

Fig. 4. Basicities (calculated with eq. 3) opposed to the actual softening behavior of bottom ashes from RK1-3 and synthesized bottom ash SYNTH. Initial diameters of bottom ash pills were 13 mm. Pills were placed on refractory material M1.

Fig. 5. Transversal cuts of examined bricks indicating the distance from the inlet [m] and remaining thicknesses [mm]. Initial thicknesses were 220 mm for M2 in RK2 and 250 mm for all other bricks.

Fig. 6. Cracks observed in every refractory and in every kiln. The yellow salt in M3 proved to be toxic potassium chromate K_2CrO_4.

Fig. 7. SEM micrographs of the refractory brick's hot face. Chemical compositions measured by EDS represent mean values of 3 measurements of the same specimen.

Fig. 8. XRF measurements at different distances from the deposit/brick interface. Refractory material M1 after 17 months in service in the combustion zone of RK2.

Fig. 9. XRF measurements at different distances from the deposit/brick interface. Refractory material M2 after 17 months in service in the outlet zone of RK2.

Fig. 10. X-ray diffraction patterns of refractory material M1 before and after use. The brick was used during 21 months in the outlet zone of rotary kiln RK1. Mineralogical phases are C-Corundum (Al_2O_3), M-Mullite ($3Al_2O_3 \cdot 2SiO_2$), Cr-Cristobalite (SiO_2) and P-Pseudobrookit (Fe_2TiO_5).

Fig. 11. X-ray diffraction patterns of refractory material M2 before and after use. The brick was used during 17 months in the outlet zone of rotary kiln RK2. Mineralogical phases are C-Corundum (Al_2O_3), M-Mullite ($3Al_2O_3 \cdot 2SiO_2$), Berlinite ($AlPO_4$), A-Andalusite ($Al_2[SiO_4]O$), E-Eskolaite (Cr_2O_3), F-Magnetite (Fe_3O_4) and G-Gehlenite ($Ca_2Al[AlSiO_7]$).

Fig. 12. X-ray diffraction patterns of refractory material M3 before and after use. The brick was used during 15 months in the outlet zone of rotary kiln RK3. Mineralogical phases are C-Corundum (Al_2O_3), E-Eskolaite (Cr_2O_3), Z-Baddeleyite (ZrO_2) and G-Gehlenite ($Ca_2Al[AlSiO_7]$).

Fig. 13. Stages of the spalling mechanism.

Fig. 14. Deposit protection and stresses in the different kiln zones. Stresses combined with poor deposit protection lead to spalling.

Tab. 1. Bottom ash compositions from rotary kiln incinerators RK1–3 and synthesized bottom ash SYNTH.
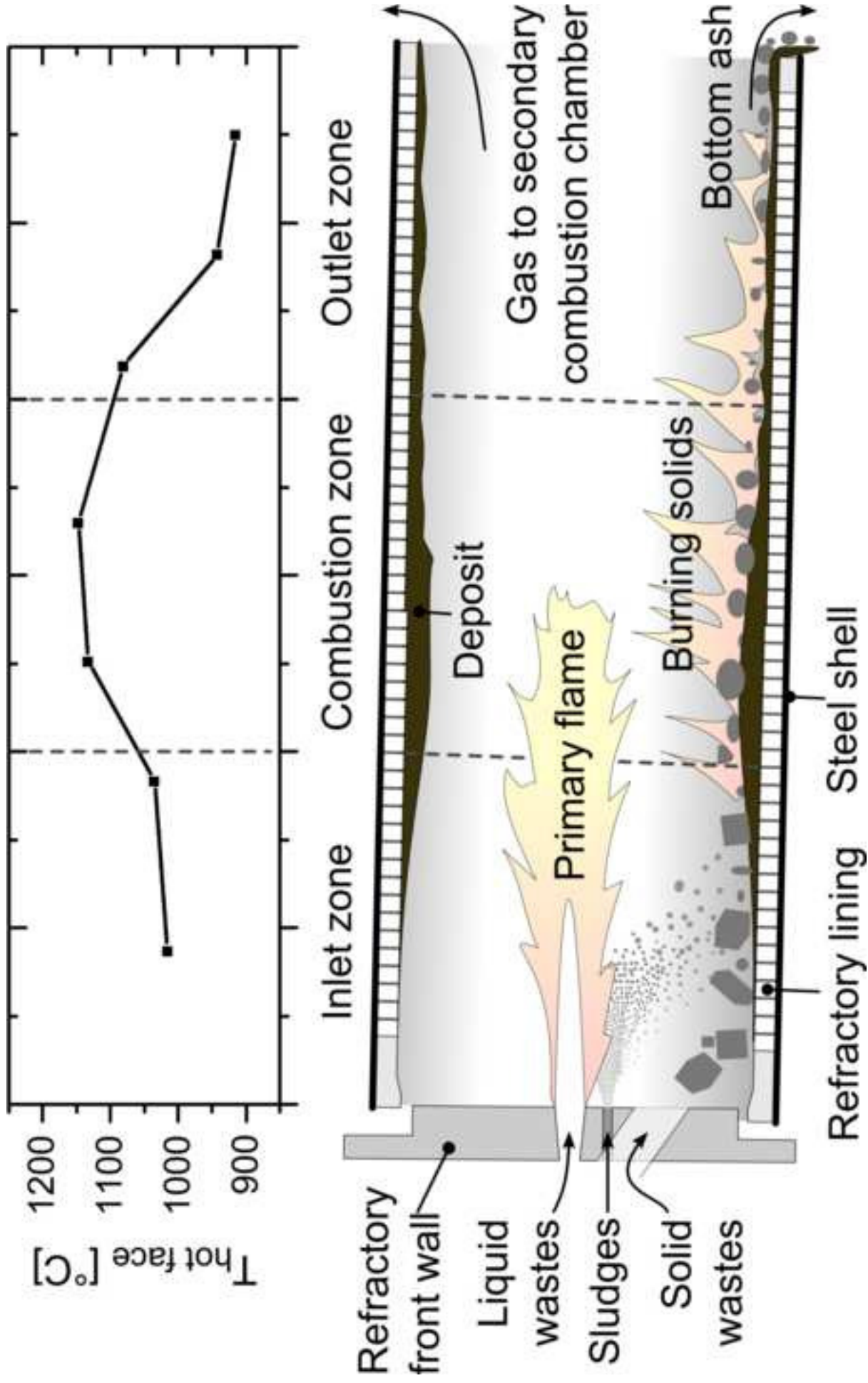
Bottom ash		RK1	RK2	RK3	SYNTH
Organic fraction		0.0	7.7	12.1	-
Composition of inorganic fraction [wt%]	Al_2O_3	6.3	6.2	14.5	10.0
	SiO_2	45.7	29.5	50.2	42.0
	P_2O_5	0.1	0.7	0.9	-
	Na_2O	2.6	4.8	6.0	8.0
	K_2O	8.4	0.9	1.7	-
	CaO	16.7	15.9	12.7	20.0
	MgO	8.1	1.5	1.8	-
	Fe_2O_3	10.2	33.5	8.2	20.0
	TiO_2	1.9	6.7	3.8	-

Tab. 2. Raw materials, mineral composition, chemical composition and properties of the refractory products as-fabricated.

Material		M1	M2	M3
Category		high alumina	alumina-chromia	alumina-chromia
Main raw materials		bauxite, clay	fused alumina, chromia, andalusite	fused alumina, chromia, AZS-aggregates
Main mineral phases		mullite, corundum	corundum, mullite, andalusite, $AlPO_4$, $(Al_2O_3\text{-}Cr_2O_3)_{ss}$	corundum, baddeleyite, $(Al_2O_3\text{-}Cr_2O_3)_{ss}$
Bonding phase		mullite	$AlPO_4$, $(Al_2O_3\text{-}Cr_2O_3)_{ss}$	$(Al_2O_3\text{-}Cr_2O_3)_{ss}$
Composition [wt%]	Al_2O_3	78	83*	84*
	SiO_2	12	10*	2*
	P_2O_5	-	2*	1*
	Fe_2O_3	3	-	-
	Cr_2O_3	-	5*	10*
	TiO_2	5	-	-
	ZrO_2	-	1*	3*
Porosity [%]		18	14	14
Average pore diameter D50 [μm]		2.1	1.3	1.7
CCS* [MPa]		95	160	180
LCTE* [°C^{-1}] (25-1000 °C)		$6.7 \cdot 10^{-6}$	$7.9 \cdot 10^{-6}$	$7.9 \cdot 10^{-6}$

*Data from technical data sheet

Figure 1
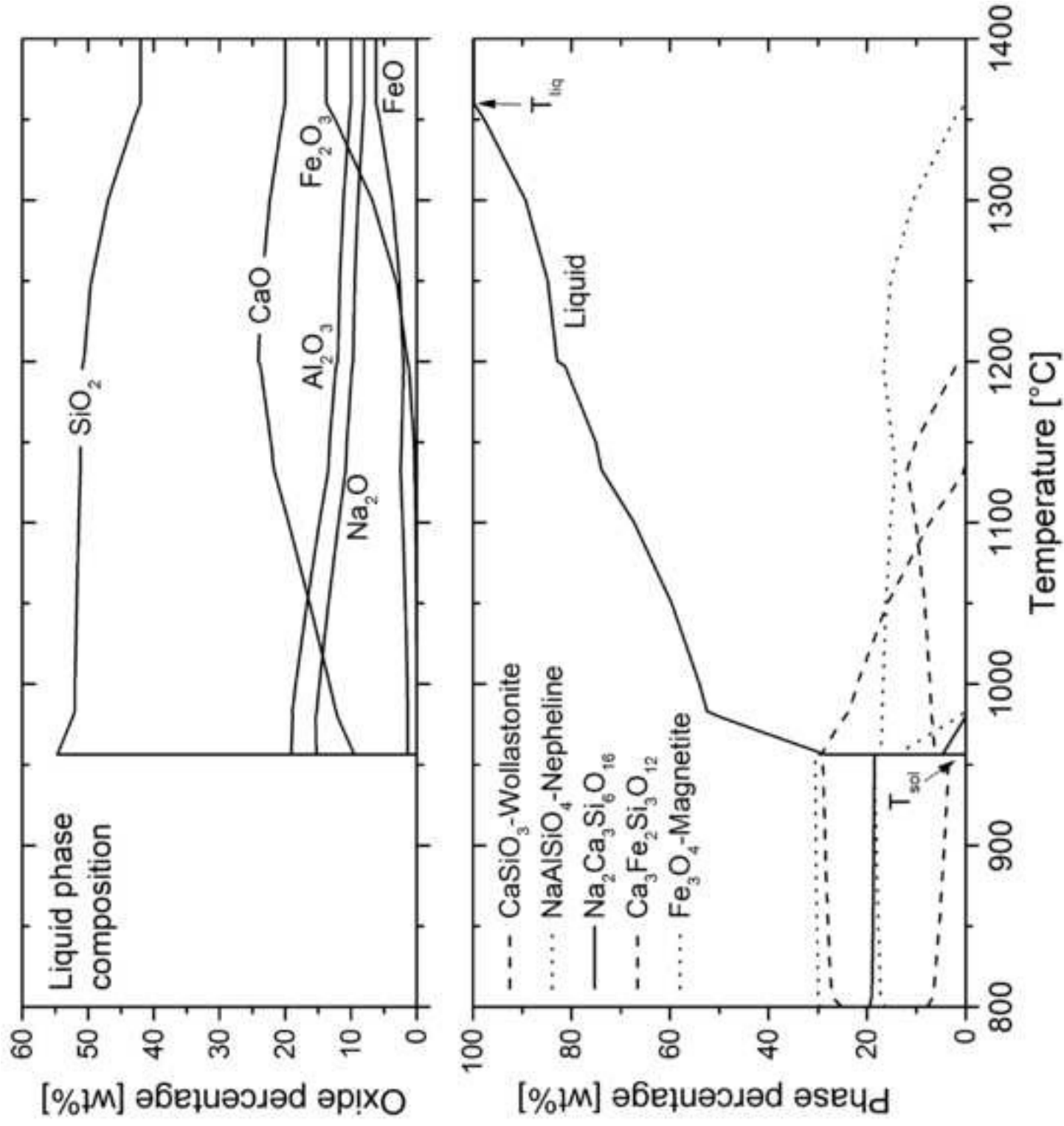
Figure 1

Figure 2

Figure 3

Figure 4

Initial
1000 °C
1050 °C
1100 °C
1150 °C

SYNTH
B=0.73

RK3
B=0.39

RK2
B=0.71

RK1
B=1.14

Figure 5

RK1

| 156 mm M1 | 157 mm M1 | 104 mm M1 | 115 mm M1 | 62 mm M1 |
| 7 m | 8 m | 10 m | 11 m | 12.3 m |

Combustion zone | Outlet zone

RK2

| 115 mm M1 | 158 mm M1 | 203 mm M1 | 183 mm M1 | 104 mm M2 | 89 mm M2 | 57 mm M2 | 59 mm M2 |
| 1.5 m | 2.5 m | 4.5 m | 5.5 m | 6.5 m | 7.5 m | 8.5 m | 9.5 m |

Inlet zone | Combustion zone | Outlet zone

RK3

| 85 mm M2 | 63 mm M2 | 43 mm M3 | 87 mm M3 |
| 3.5 m | 4.5 m | 5.5 m | 6.5 m |

Combustion zone | Outlet zone

Figure 6

Deposit of solidified bottom ash

Cracks

Cracks

Cracks

Potassium chromate

M1
Outlet zone RK1

M2
Outlet zone RK2

M3
Outlet zone RK3

10 mm

10 mm

10 mm

Figure 7

EDS [wt%]	Al_2O_3	SiO_2	Na_2O	K_2O	CaO	MgO	Fe_2O_3	TiO_2
Deposit	7.2	39.8	3.4	5.1	19.9	4.2	15.4	5.0
Infiltrating liquid	6.5	47.1	3.7	7.0	20.1	5.8	7.8	2.0

M1, outlet zone RK1

M2, outlet zone RK2

Bauxite aggregate

Corundum aggregate

Micro-cracks in matrix

Infiltrated cracks and pores

Macro-crack

Deposit

Distance from deposit/brick interface [mm]

Figure 8

Figure 9

Figure 10
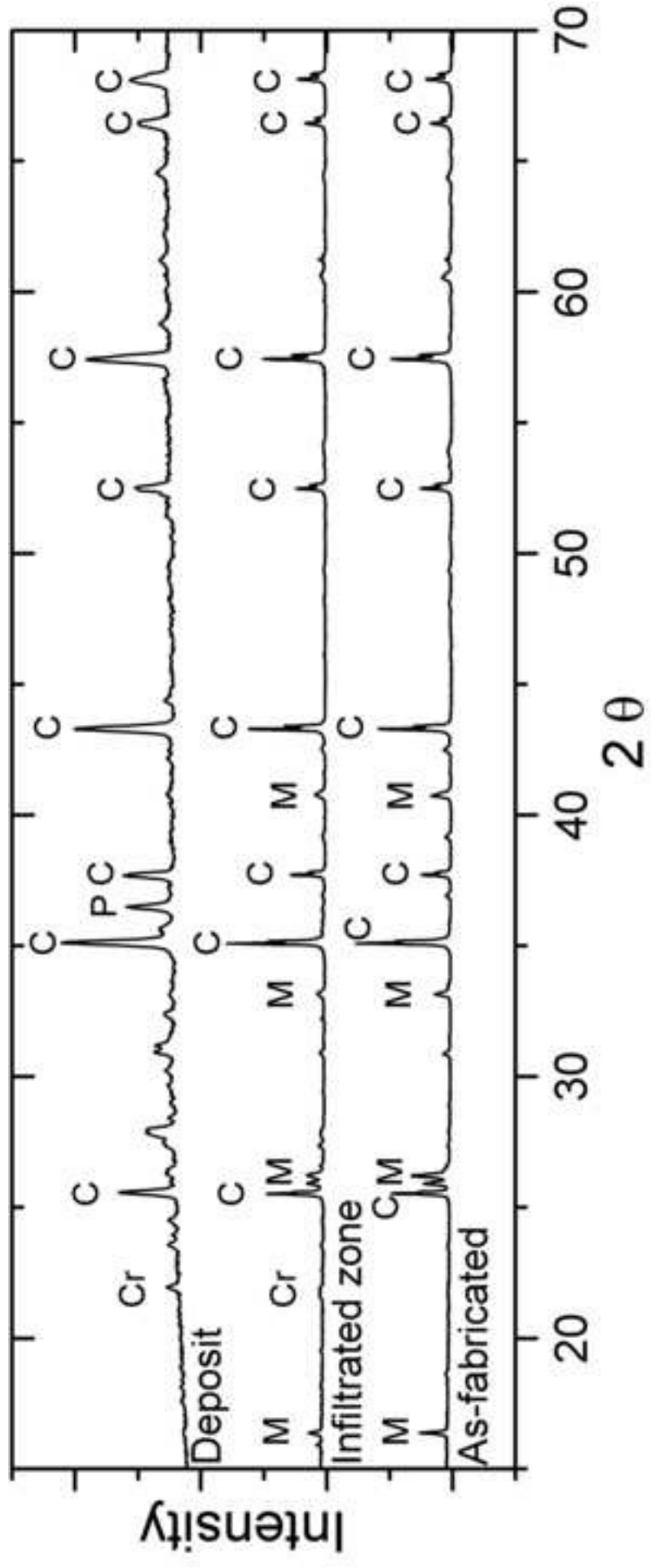
Figure 11

Figure 12

Figure 13

Deposit — Infiltration and crack formation — 20 mm

Deposit — Crack growth — 20 mm

Deposit — Spalling — 20 mm

Figure 14